Journal of Alloys and Compounds 530 (2012) 48–55

Contents lists available at SciVerse ScienceDirect

Journal of Alloys and Compounds

journal homepage: www.elsevier.com/locate/jallcom

Effects of equal channel angular extrusion on the microstructure and high-temperature mechanical properties of ZA85 magnesium alloy

Che-Yi Lin, Hao-Jan Tsai, Chuen-Guang Chao*, Tzeng-Feng Liu

Department of Materials Science and Engineering, National Chiao Tung University, 1001 Ta Hsueh Road, Hsinchu 30050, Taiwan

ARTICLE INFO

Article history:
Received 29 September 2010
Received in revised form 23 March 2012
Accepted 26 March 2012
Available online 3 April 2012

Keywords:
Equal channel angular extrusion
ZA85 magnesium alloy
Microstructure
High-temperature mechanical properties

ABSTRACT

This study examined the microstructure and high-temperature tensile properties of the Mg–8 wt.%Zn–5 wt.%Al (ZA85) alloy that was subjected to equal channel angular extrusion (ECAE) with various passes at 180–250 °C. The original grain size and precipitate size of the as-cast specimen were 150 and 100 μm, respectively. The average grain size was reduced to 4 μm by dynamic recrystallization and the precipitate size was reduced to 1 μm after six ECAE passes at 180 °C. However, the average grain size of the ECAE-processed specimens at 250 °C increased from 14 μm after two passes to 20 μm after four passes owing to the grain growth effect. In tensile tests at 200 °C, the ultimate tensile strength (UTS) and yield strength (YS) of the specimens processed with six ECAE passes at 180 °C improved to 249 MPa and 162 MPa, respectively, compared with 105 MPa (UTS) and 74 MPa (YS) for the as-cast specimens. Furthermore, elongation increased from 5.1% to 28.5%. This significant improvement in the high-temperature tensile properties of the ZA85 alloy was attributed to the refined grains and the well-distributed fine $Mg_{32}(Al, Zn)_{49}$ (τ-phase) precipitates.

1. Introduction

In recent years, the development of magnesium alloys, which generally have excellent properties such as low density, high specific strength, superior damping capacity, high thermal conductivity, and good electromagnetic shielding characteristics, has been attracting much attention [1–4]. These properties make magnesium alloys suitable for a broad range of applications in electronic devices and the aircraft and automobile industries among others. Among various magnesium alloys, Mg–Al–Zn (AZ) alloys are widely used because of their desirable mechanical properties, corrosion resistance, and castability. However, the application of these alloys is limited at temperatures above 120 °C. This is because their heat resistance is inferior to that of aluminum alloys at high temperatures [5]. This phenomenon is attributed to the presence of intermetallic $Mg_{17}Al_{12}$ (β-phase), which mainly precipitates along grain boundaries and exhibits a low decomposition temperature of approximately 470 °C. Thus, grain boundary sliding occurs even at temperatures below 150 °C [6,7]. It has been reported that the addition of rare earth (RE) elements to magnesium improves its properties at elevated temperatures [8–10]. However, the use of Mg–RE alloys is limited owing to their inferior ductility and the high cost of RE elements. Another way to improve the high-temperature performance of AZ alloys is to suppress the formation of the β-phase [11]. It has been reported that a ternary addition of a large amount of zinc to binary Mg–Al alloys, with a Zn:Al composition of approximately 2:1, can completely suppress the formation of the β-phase [12,13]. The main precipitate of Mg–Zn–Al (ZA) alloys is $Mg_{32}(Al, Zn)_{49}$ (τ-phase), which has a higher melting point and decomposition temperature than the β-phase [14]; therefore, ZA alloys exhibit better properties at elevated temperatures compared with commercial AZ alloys.

Another disadvantage of commercial magnesium alloys is their poor formability and low ductility at room temperature (RT) as a result of their hexagonal close-packed (HCP) crystal structure, which limits their practical applications. Microstructure refinement is a promising method to increase the ductility and strength of magnesium alloys. Severe plastic deformation (SPD) has been introduced in materials processing to produce ultrafine-grained microstructures [15]. Equal channel angular extrusion (ECAE) is one of the most popular SPD methods and can produce a homogeneous submicron or nanocrystalline microstructure in bulk materials [16,17]. A block with two intersecting channels that have identical cross sections is used as an ECAE die. Severe deformation occurs via simple shear in the zone where the two channels intersect. Large amounts of strain can accumulate by repeated pressing because the channel cross sections are identical. ECAE is proven to be effective in refining grains in various magnesium alloys, resulting in improved ductility, strength, and superplasticity [18–22].

* Corresponding author. Tel.: +886 3 5731809; fax: +886 3 5724727.
E-mail addresses: cgchao@mail.nctu.edu.tw, cylin0207.mse96g@g2.nctu.edu.tw (C.-G. Chao).

0925-8388/$ – see front matter © 2012 Elsevier B.V. All rights reserved.
http://dx.doi.org/10.1016/j.jallcom.2012.03.107

ECAE research on Mg alloys has focused mainly on AZ alloys. The effects of ECAE on ZA alloys, which have better high-temperature properties compared with AZ alloys, have not been investigated yet. Therefore, we investigate the microstructure and tensile properties of the as-cast ZA85 alloy after ECAE via route B_C [23] at 180, 220, and 250 °C.

2. Experimental details

The experimental alloy was prepared from commercially pure Mg, Al, and Zn (>99.9%). A steel crucible and an electron resistance furnace were used for melting and alloying with SF_6 as the protective atmosphere. Steel molds were used for casting the alloy. The as-cast alloy was air cooled from the molten state. The chemical composition of the experimental alloy was determined by energy dispersive spectroscopy. The results of chemical analyses were averaged over three different regions that were chosen randomly from the ingot. The chemical composition of the alloy is 8.34 wt.% Zn, 4.74 wt.% Al with the balance Mg. For ECAE, specimens of dimensions 17 mm × 17 mm × 60 mm were cut from the ingot, and an ECAE die with an angle of 120° was used. Boron nitride was used as the lubricant during ECAE. The ECAE die was preheated to 180, 220, and 250 °C and maintained for 15 min before inserting a lubricated ECAE specimen into the entrance channel. All specimens were held inside the ECAE die for 5 min before pressing. These specimens were processed via route B_C in which after each pass, the specimen was rotated through 90° in the same direction at a pressing speed of 2 mm/min. Microstructures of the as-cast and ECAE materials were examined by standard metallographic procedures. The polished surface was etched with 3 mL acetic acid solution, 5 mL deionized water, 35 mL ethanol, and 1 g picric acid. The microstructures were observed by optical microscopy, scanning electron microscopy (SEM), and transmission electron microscopy (TEM). Regarding the ECAE specimens, the surfaces perpendicular to ND (*y*-plane) were observed [24]. The average grain size, grain size distribution, and area fraction of grain size were obtained with Image Pro software (IpWin32). A Rockwell indenter with a load of 100 kgf was used for a Rockwell hardness B (HRB) test at RT. The HRB values were averaged over 10 tests under each condition. The ECAE specimens were longitudinally cut to obtain tensile specimens with a gauge section of 6 mm × 3 mm × 2 mm. Tensile tests were conducted at RT and 200 °C with an initial strain rate of 1×10^{-3} s^{-1} using an Instron 8501 universal testing machine. An electric furnace mounted on the machine was used for high-temperature tensile tests. The specimens were heated to 200 °C and then held for 10 min prior to the tensile tests. Ultimate tensile strength (UTS), yield strength (YS), and elongation were averaged over three to five tests under each condition.

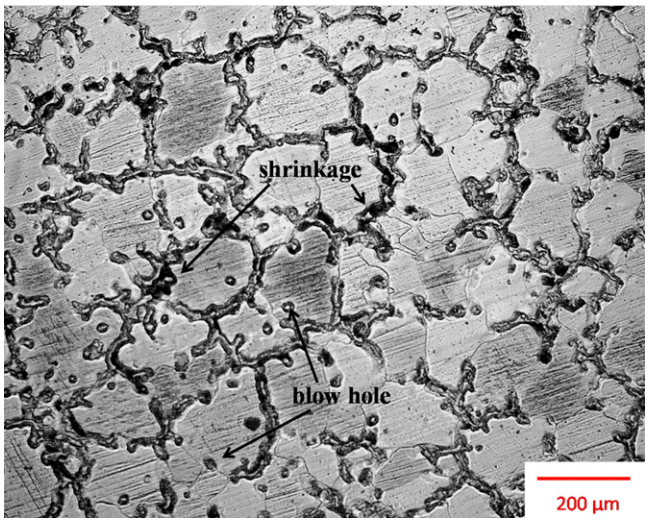

Fig. 1. Optical micrograph of the as-cast ZA85 alloy.

3. Results

3.1. Microstructure

The optical micrograph of the as-cast ZA85 alloy shows an equiaxed grain structure with an average grain size of approximately 150 μm, as shown in Fig. 1. The coarse precipitates, identified as the τ-phase by X-ray diffraction (the same as in prior literatures [12,14,25]), are distributed along the grain boundaries.

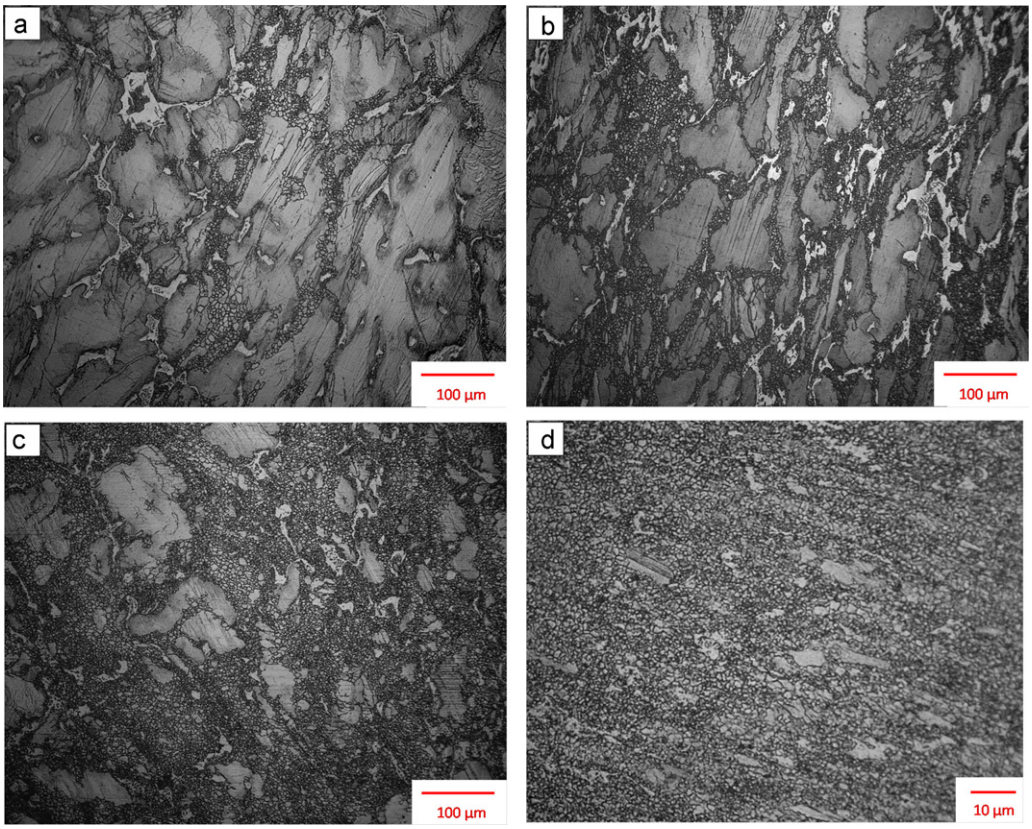

Fig. 2. Optical micrographs of the ZA85 alloy after ECAE at 180 °C for (a) *N* = 1, (b) *N* = 2, (c) *N* = 4, and (d) *N* = 6.

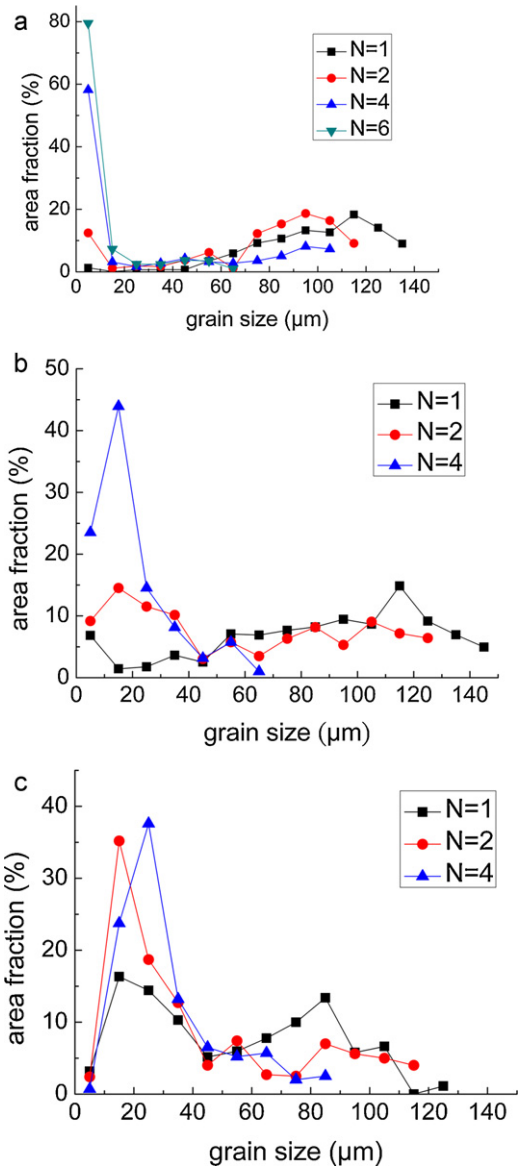

Fig. 3. Area fraction of grains with different sizes after ECAE at (a) 180 °C, (b) 220 °C, and (c) 250 °C.

Moreover, several defects such as blow holes and shrinkage voids can be clearly observed in the as-cast specimen. These defects result from the air trapped in the melting alloy during casting and from the difference between the cooling rates in the inner and outer regions of the ingot.

3.1.1. Effect of the number of ECAE passes on microstructure

Fig. 2 shows the optical micrographs of the ECAE-processed specimens after different number of passes were conducted at 180 °C. After fewer than four ECAE passes, all microstructures became inhomogeneous with fine recrystallized grains along the grain boundaries and a number of large distorted grains. This resultant microstructure, termed as "bimodal", was also observed by Chang et al. [26]. Fig. 2(d) shows that after six ECAE passes, the microstructure became visibly uniform, and the average grain size was significantly reduced to approximately 4 μm. In addition, the microstructures existed in a preferential orientation after one, two, and six passes but not after four passes.

Fig. 3 shows the area fraction of grain sizes for the ECAE-processed specimens. As can be observed in Fig. 3(a), the area fraction of fine grains (less than 10 μm) increased with the number of ECAE passes at 180 °C. This indicates that the area fraction of dynamically recrystallized grains progressively increased with strain. In addition, the area fraction of large grains apparently decreased with subsequent passes. This suggests that ECAE can result in a uniform microstructure. Furthermore, defects such as blow holes and shrinkage voids in the as-cast specimen were eliminated after ECAE, as shown in Fig. 2.

The SEM micrographs (Fig. 4) show the effect of ECAE on the precipitates. The precipitate size reduced with increasing number of ECAE passes. After four passes, the size was significantly reduced to less than 10 μm. After six passes, it was further reduced to an average of 1 μm with uniform distribution.

Fig. 5 shows a TEM micrograph of the ECAE-processed ZA85 alloy at 180 °C after six passes. It can be observed that there were several dislocation-free grains approximately 1 μm in size. However, a few grains contained dislocations due to excessive strain during ECAE. The darker particles in Fig. 5 are the precipitates, which were distributed uniformly in the material.

3.1.2. Effect of ECAE temperature on the microstructure

Figs. 6 and 7 show the optical micrographs of the ECAE specimens after different number of passes at 220 and 250 °C, respectively. Compared to the results at the lower ECAE temperature of 180 °C, the degree of dynamic recrystallization increased with ECAE temperature so that a more uniform microstructure was obtained at higher temperatures. Figs. 6(c) and 7(c) show that the microstructures obtained after four ECAE passes at 220 and 250 °C were more uniform than those at 180 °C. These new fine grains grew slightly during ECAE at 220 and 250 °C. The area fraction of grains less than 10 μm in size reached 80% after six passes at 180 °C. On the other hand, most of the dynamically recrystallized grains had grown to 10–20 μm during ECAE at 220 °C, as shown in Fig. 3(b). The area fraction of grains of sizes 10–20 μm was approximately 1.5% after one pass and increased to approximately 14.5% and 44% after two and four passes, respectively. After ECAE at 250 °C, grain growth was more evident. In particular, most of the dynamically recrystallized grains had grown to sizes 20–30 μm, as shown in Fig. 3(c). Furthermore, the area fraction of grains with sizes 20–30 μm increased to approximately 38% after four passes.

Fig. 8 shows the average grain size with different number of ECAE passes at different temperatures. It can be observed that the degree of grain refinement increased with ECAE temperature after one pass. The average grain sizes of the specimens were 31, 19, and 16 μm after one pass at 180, 220, and 250 °C, respectively. However, the grain refinement rate decreased with additional passes at 220 °C. Note that the average grain size increased from 14 μm after two passes to 20 μm after four passes at 250 °C. In contrast, at the lower ECAE temperature of 180 °C, the average grain size reduced to 8 μm after four ECAE passes. It could be further reduced to 4 μm after six ECAE passes without conspicuous grain growth.

3.2. Mechanical properties

Fig. 9 shows the results of a hardness test on the ZA85 alloy at RT with different number of ECAE passes at different ECAE temperatures. Grain size is inversely proportional to hardness. Hardness increased with the number of passes at 180 and 220 °C. However, hardness increased to HRB 31 after two passes but decreased to HRB 27 after four passes because of the apparent grain growth effect at 250 °C. Moreover, hardness increased significantly from HRB 19 to HRB 46 after six passes at 180 °C.

Fig. 10 shows the results of the tensile tests on the ZA85 alloy conducted at RT. The tensile properties were similar to the hardness properties. For the as-cast specimen, UTS was 175 MPa at RT. After one ECAE pass at 180, 220, and 250 °C, UTS increased to 187,

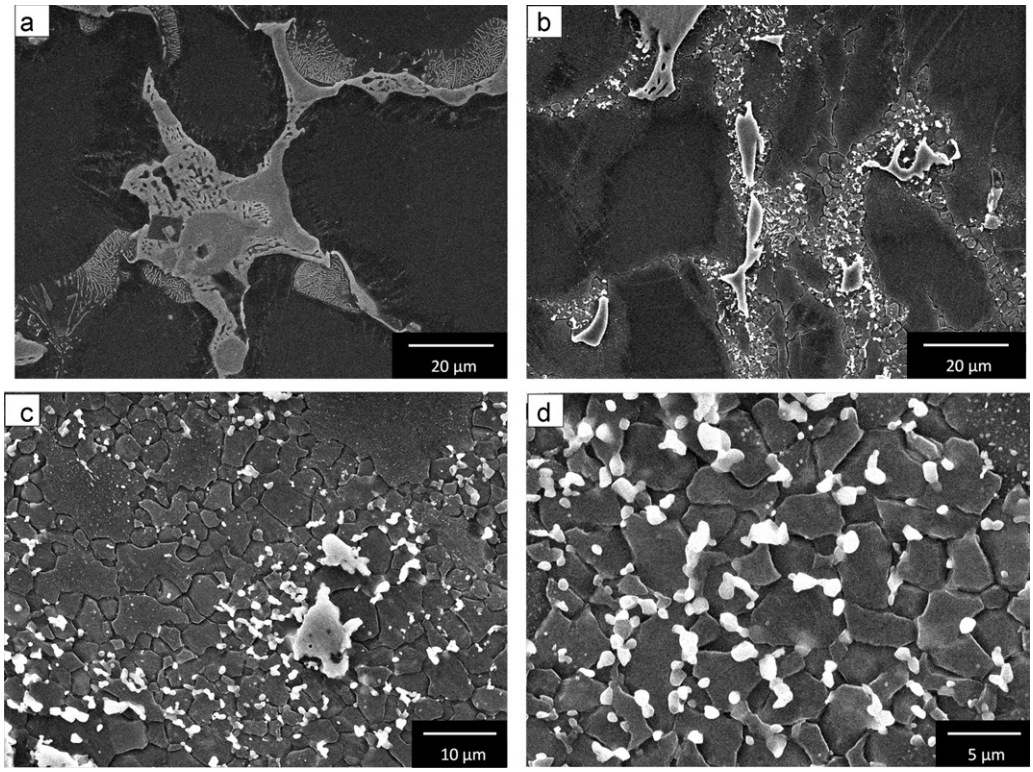

Fig. 4. SEM micrographs of the ZA85 alloy after ECAE at 180 °C for (a) $N = 0$, (b) $N = 1$, (c) $N = 4$, and (d) $N = 6$.

198, and 220 MPa, respectively. It can be observed that ECAE temperature varies directly with the strength of the alloy. In addition, UTS and YS increased with additional ECAE passes at 180 and 220 °C but decreased with increasing number of ECAE passes from two to four; this is owing to the grain growth effect at 250 °C. At 180, 220, 250 °C, the UTS of the four-pass ECAE-processed specimens were 373, 348, and 242 MPa, respectively. At 180 °C, the UTS of the six-pass ECAE-processed specimens reached 402 MPa. Compared with those of the as-cast ZA85 alloy, the UTS and YS at RT were improved by up to 230% and 215%, respectively. The tensile properties at RT in the present study are also superior to those of many other AZ series alloys that were subjected to ECAE, as shown in Table 1 [18,27–29].

Fig. 10(c) shows that the elongation of the present alloy at RT was improved by ECAE. After six passes at 180 °C, the elongation of the alloy improved from 2.3% to approximately 6.4%.

Fig. 11 shows the results of the high-temperature tensile tests conducted at 200 °C. The high-temperature tensile properties were similar to the RT properties. The UTS and YS of six-pass ECAE-processed specimens increased to 249 and 162 MPa at 200 °C, respectively. Compared with the 105 and 74 MPa values of the as-cast ZA85 alloy, the UTS and YS at 200 °C were improved by up to 229% and 210%, respectively. Note that the high-temperature tensile properties of the ZA85 alloy in the present study are superior to those of other high-temperature magnesium alloys, as shown in Table 2 [30]. In addition, elongation increased to 28.5% in the tensile test at 200 °C after six ECAE passes at 180 °C.

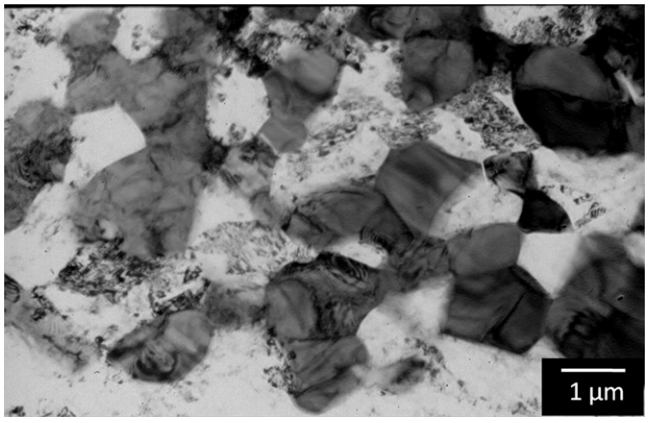

Fig. 5. TEM micrograph of the ZA85 alloy after six-pass ECAE at 180 °C.

4. Discussion

After ECAE at 180 °C with less than four passes, the optical micrographs show a bimodal microstructure, as shown in Fig. 2(a)–(c). These differ from the microstructure of aluminum alloys subjected to ECAE. Nakashima et al. [31] reported that after two ECAE passes at RT, the microstructure of aluminum alloys became homogeneous with ultrafine grains less than 1 μm in size. This phenomenon is attributed to the difference between the grain refinement mechanisms of magnesium and aluminum alloys. For aluminum alloys, Berbon and Langdon [32] proposed a grain refinement mechanism during ECAE deformation. In the first pass, several dislocations are introduced within the grain because of the applied strain. These dislocations then rearrange into low-energy dislocation structures (LEDSs). The dislocations generated in the following passes then transform the LEDSs into subgrains. With increasing number of ECAE passes, boundary misorientation would increase to form high-angle grain boundaries. However, the grain refinement mechanism of magnesium alloys by ECAE is mainly dynamic recrystallization [28,33] because of the relatively few slip systems in HCP metals during ECAE at testing temperatures. In HCP metals, the slip system at RT is mainly the basal slip system. At high temperatures, non-basal slip systems such as prismatic and pyramidal slip systems can become activated. However, in this study, ECAE processing temperatures are below 250 °C, which is not

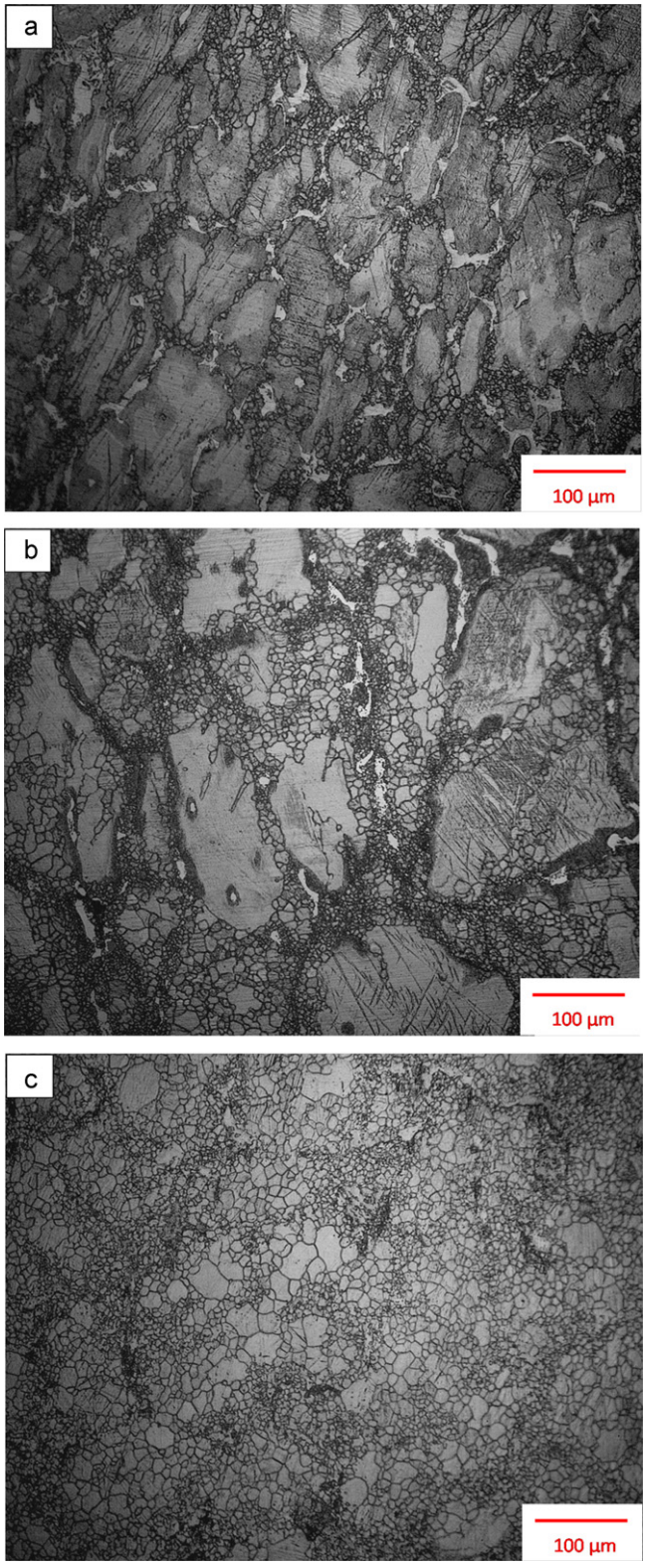

Fig. 6. Optical micrographs of the ZA85 alloy after ECAE at 220 °C for (a) $N = 1$, (b) $N = 2$, and (c) $N = 4$.

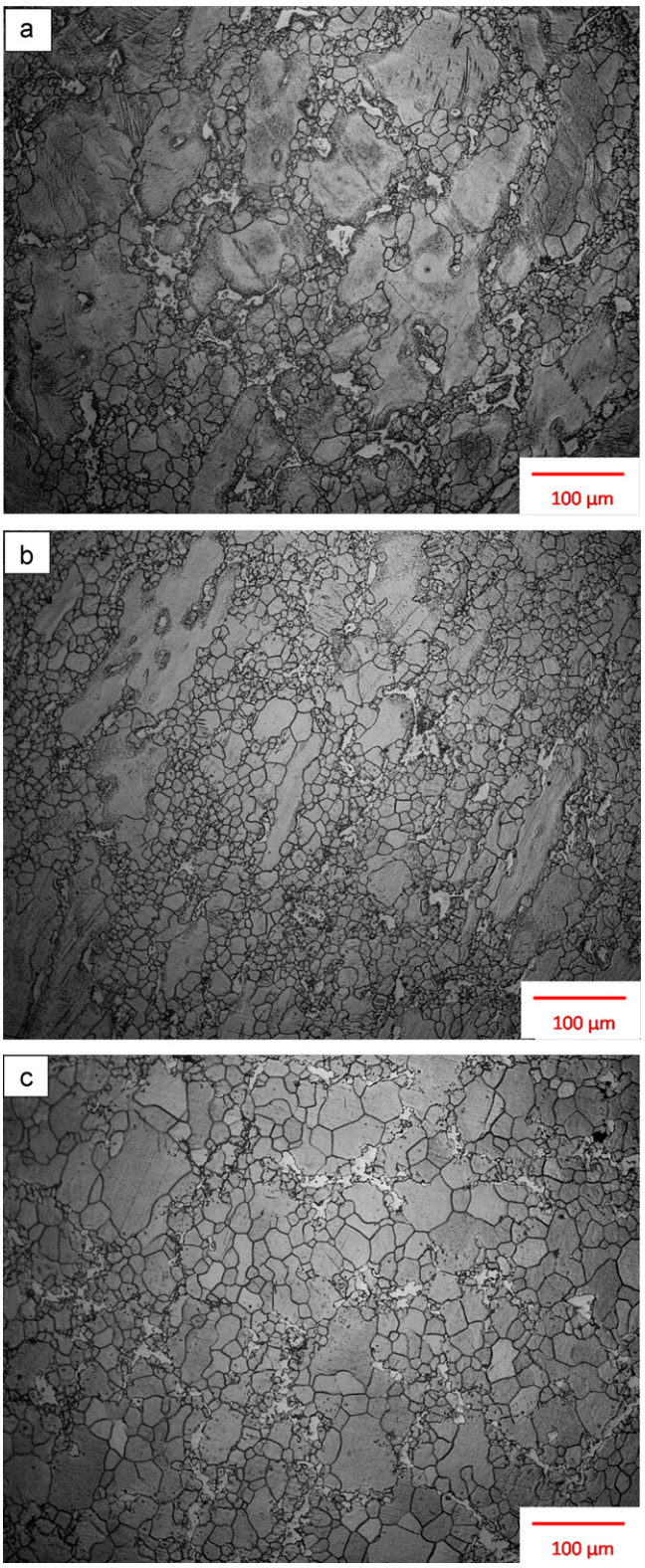

Fig. 7. Optical micrographs of the ZA85 alloy after ECAE at 250 °C for (a) $N = 1$, (b) $N = 2$, and (c) $N = 4$.

sufficiently high to activate all non-basal slip systems [34]. Therefore, dynamic recrystallization is responsible for grain refinement. From the TEM micrograph shown in Fig. 5, it can be observed that after six ECAE passes at 180 °C, there are several dislocation-free grains attributable to dynamic recrystallization. The density of dislocation increases owing to the large amount of strain accumulated by the repetition of ECAE processes. Then, dynamic recrystallization occurs in the area of high dislocation density, producing numerous fine grains and reducing dislocation density. It should be noted that the microstructures exist in a preferential orientation after one, two, and six passes but not after four passes. In this study, because ECAE is conducted via route B_C, in which the specimen is rotated

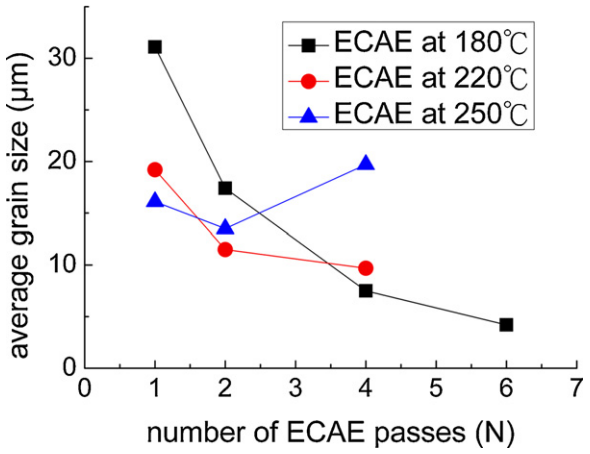

Fig. 8. Average grain size with number of passes at different ECAE temperatures.

90° in the same direction after each pass, the grain structure would return to an equiaxed structure after every four passes.

Fig. 4 shows that the size of the precipitates decreases with increasing number of ECAE passes. This proves that ECAE not only reduces grain size but also shatters coarse precipitates. In general, the precipitates shattered by shear stress during ECAE ought to have an irregular shape and a rough surface. In this study, ECAE is conducted at high temperatures with a low pressing speed; hence, the precipitate surface becomes smoother to reduce surface energy.

Figs. 6(c) and 7(c) show that the microstructures after four ECAE passes at 220 and 250 °C are more uniform than the microstructure after four ECAE passes at 180 °C. This indicates that a higher temperature is more beneficial for dynamic recrystallization. Therefore, the degree of dynamic recrystallization increases with ECAE temperature, leading to much more uniform microstructures at higher ECAE temperatures with the same number of ECAE passes. Note that the average grain size increases from 14 μm after two passes to 20 μm after four passes at 250 °C. On the other hand, at the lower ECAE temperature of 180 °C, the average grain size reduces to 4 μm after six passes without conspicuous grain growth. Grain growth occurs during ECAE owing to the high temperature.

Fig. 9 shows that hardness increases with the number of ECAE passes, which can be attributed to two factors. The first one is grain refinement. As can be observed in Figs. 8 and 9, a smaller grain size is accompanied by greater hardness. The second factor is the

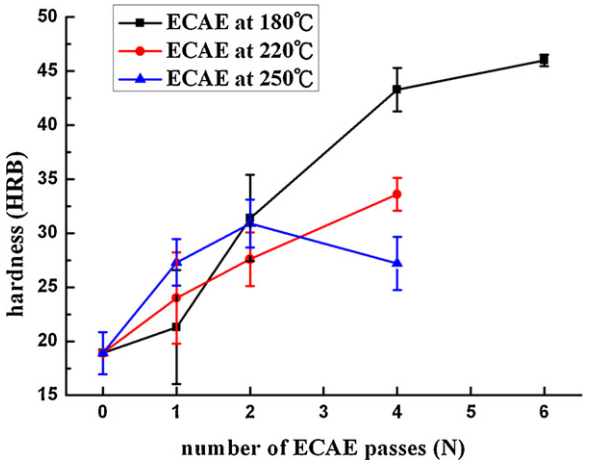

Fig. 9. Hardness at room temperature with different number of passes at different ECAE temperatures.

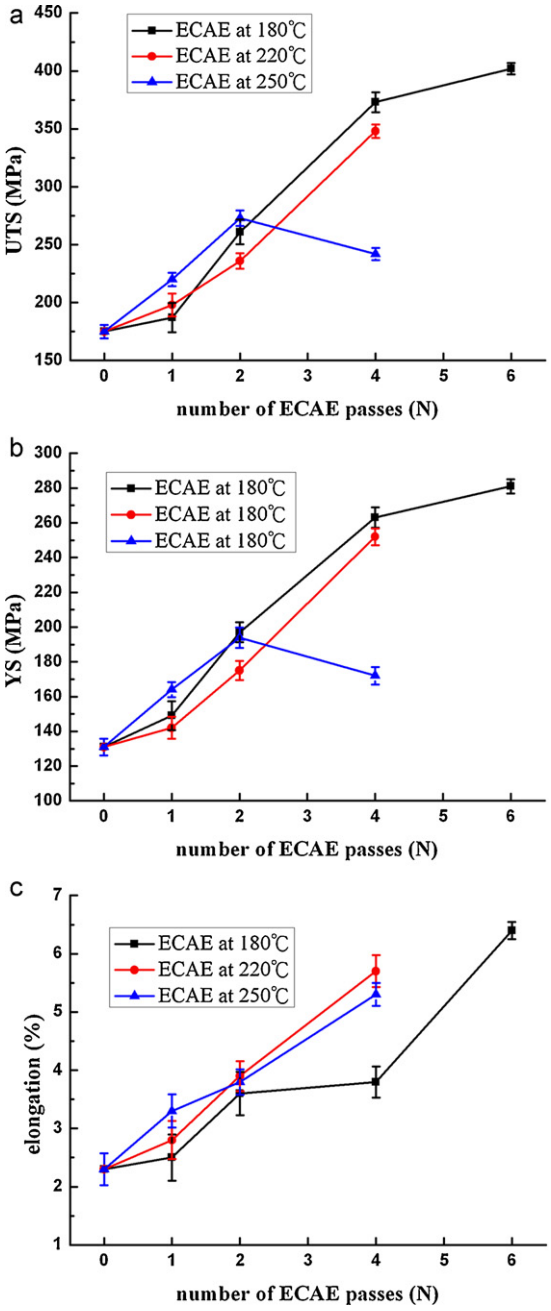

Fig. 10. Tensile properties at room temperature: (a) UTS, (b) YS, and (c) elongation.

shattered precipitates. These uniformly distributed fine precipitates would hinder grain boundary sliding as well as dislocation slips, which leads to better mechanical properties.

Fig. 10(a) and (b) shows the UTS and YS properties, respectively, of the ZA85 alloy at RT. The tensile properties are similar to the hardness properties. Fig. 10(c) shows that the elongation of this alloy at RT is improved by ECAE. This increment in elongation is attributed to (1) the elimination of defects such as blow holes and shrinkage voids formed during casting, as shown in Fig. 2, and (2) precipitate refinement. It is worth mentioning that after four ECAE passes, the average grain size at 180 °C is smaller than that at 250 °C, whereas elongation is higher in the latter case. This phenomenon can be attributed to the degree of dynamic recrystallization during ECAE. As can be observed in Fig. 2(c), after four ECAE passes at 180 °C, the microstructure is rather inhomogeneous with fine recrystallized grains as well as a number of large initially distorted

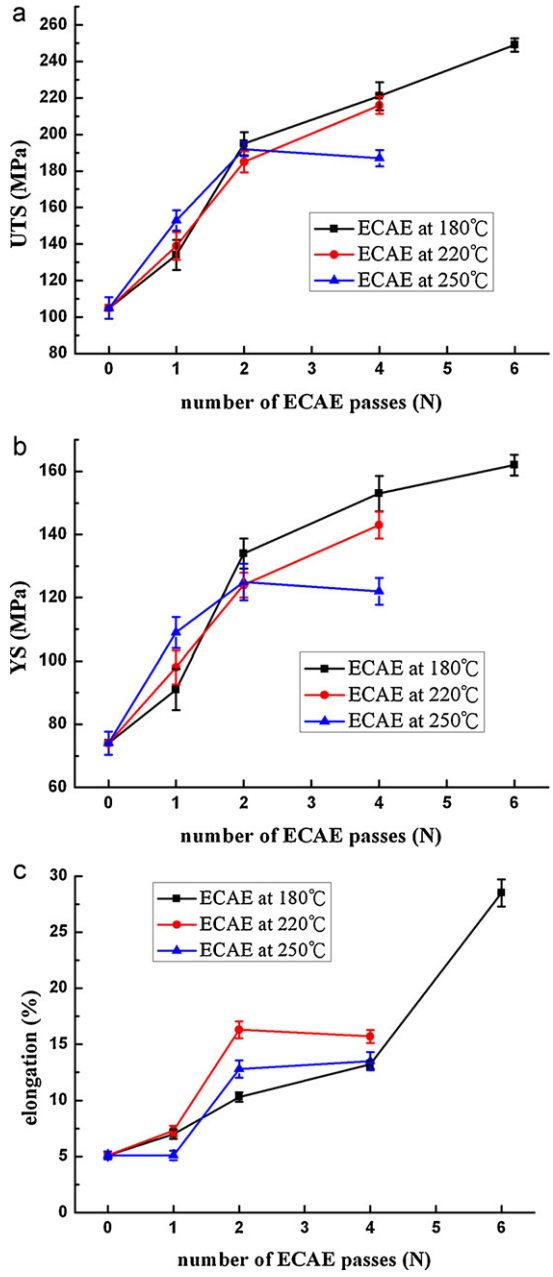

Fig. 11. Tensile properties at 200 °C: (a) UTS, (b) YS, and (c) elongation.

grains. On the other hand, the microstructure is more uniform with fully recrystallized grains after four ECAE passes at 250 °C, as shown in Fig. 7(c). Therefore, the dislocation density due to ECAE would be considerably reduced by the high degree of recrystallization in the latter case, thereby leading to a material with higher ductility.

The high-temperature tensile properties of materials are influenced by several factors such as average grain size and precipitate size as well as their distribution. In the present study, it is evident that the grains and precipitates are significantly refined and well distributed by ECAE, as shown in Figs. 4(d) and 5(b). In this study, the improvement in high-temperature tensile properties is mainly attributed to the refined grains and precipitates. After ECAE, both coarse grains and precipitates with initial sizes greater than 100 μm are considerably refined to less than 10 μm. According to the deformation mechanism map of pure magnesium, the high-temperature deformation of the present experimental condition could be termed as dislocation glide. Therefore, we assume that

Table 1
Room temperature tensile properties of the ZA85 alloy.

Alloy	Condition	UTS (MPa)
AZ91	Die-cast, $N = 8$	375 [18]
AZ31	As-extruded, $N = 8$	310 [27]
AZ31	SC[b], $N = 4$	210 [28]
AZ31	HR[c], $N = 4$	350 [29]
ZA85[a]	As-cast, $N = 6$	402

[a] This work.
[b] Squeeze casting.
[c] Hot rolling.

Table 2
High-temperature tensile properties of the ZA85 alloy [29].

Alloy	Temperature (°C)	UTS (MPa)
AE42	177	135
AX53	175	196
AJ52X	175	148
AXJ	175	196
ZA85[a]	200	249

[a] This work.

the deformation of the ZA85 alloy during the high-temperature tensile tests is dislocation glide. Consequently, the refined grains less than 10 μm in size would hinder dislocation to improve the high-temperature properties. Moreover, the precipitates also play an important role in improving the high-temperature properties. The refined precipitates uniformly distributed at grain boundaries hinder grain boundary migration. The precipitate of the ZA85 alloy is the τ-phase instead of the β-phase, which is the main precipitate of commercial AZ series alloys. The τ-phase has a higher decomposition temperature than the β-phase. Therefore, the significant improvement in the high-temperature tensile properties of the ZA85 alloy after ECAE is ascribed to the well-distributed τ-phase.

5. Conclusions

The effects of ECAE on the microstructure and high-temperature tensile properties of the ZA85 magnesium alloy were examined, and some interesting findings were obtained.

(1) The original grain size under the as-cast condition (about 150 μm) was significantly reduced to 4 μm after six ECAE passes at 180 °C. On the other hand, the average grain size of the ECAE-processed specimens at 250 °C increased from 14 μm after two passes to 20 μm after four passes owing to the grain growth effect. At first, the microstructure was not uniform, showing a "bimodal" grain size distribution; however, it became more homogeneous with further ECAE passes.
(2) The hardness at RT increased with the number of ECAE passes; this can be attributed to grain refinement and the shattered precipitates that were distributed uniformly in the material. Furthermore, hardness increased from HRB 19 to HRB 46 after six passes at 180 °C.
(3) The precipitate size was significantly reduced, from an average of 100 μm to 1 μm, with increasing number of ECAE passes and uniform distribution was obtained after six passes.
(4) In RT tensile tests, the UTS, YS, and elongation of the as-cast ZA85 alloy were 175 MPa, 130 MPa, and 2.3%, respectively. After six passes at 180 °C, UTS, YS, and elongation increased to 402 MPa, 281 MPa, and 6.4%, respectively.
(5) Tensile tests at an elevated temperature of 200 °C showed that the UTS, YS, and elongation of the as-cast ZA85 alloy were 105 MPa, 74 MPa, and 5.1%, respectively. After six ECAE passes at 180 °C, UTS, YS, and elongation increased to 249 MPa, 162 MPa, and 28.5%, respectively. Therefore, the

high-temperature tensile properties of the present alloy are superior to those of many other commercial high-temperature magnesium alloys.

Acknowledgment

The authors are pleased to acknowledge the financial support of this research by the National Science Council, Republic of China under Grant NSC96-2221-E-009-099.

References

[1] D.J. Li, X.Q. Zeng, J. Dong, C.Q. Zhai, W.J. Ding, Journal of Alloys and Compounds 468 (2009) 164–169.
[2] M. Bamberger, G. Dehm, Annual Review of Materials Research 38 (2008) 505–533.
[3] X.F. Huang, W.Z. Zhang, J.F. Wang, W.W. Wei, Journal of Alloys and Compounds 516 (2012) 186–191.
[4] K. Liu, J. Meng, Journal of Alloys and Compounds 509 (2011) 3299–3350.
[5] D.H. Xiao, M. Song, F.Q. Zhang, Y.H. He, Journal of Alloys and Compounds 484 (2009) 416–421.
[6] A. Srinivasan, U.T.S. Pillai, B.C. Pai, Metallurgical and Materials Transactions 36A (2005) 2235–2243.
[7] B.H. Kim, S.W. Lee, Y.H. Park, I.M. Park, Journal of Alloys and Compounds 493 (2010) 502–506.
[8] I.A. Anyanwu, Y. Gokan, S. Nozawa, A. Suzuki, S. Kamado, Y. Kojima, S. Takeda, T. Ishida, Materials Transactions 44 (2003) 562–570.
[9] J.F. Nie, K. Oh-ishi, X. Gao, K. Hono, Acta Materialia 56 (2008) 6061–6076.
[10] D. Wu, R.S. Chen, E.H. Han, Journal of Alloys and Compounds 509 (2011) 2856–2863.
[11] H. Liu, Y. Chen, Y. Tang, S. Wei, G. Niu, Journal of Alloys and Compounds 440 (2007) 122–126.
[12] Z. Zhang, A. Couture, A. Luo, Scripta Materialia 39 (1998) 45–53.
[13] M. Vogel, O. Kraft, E. Arzt, Scripta Materialia 48 (2003) 985–990.
[14] J. Zhang, Z.X. Guo, F. Pan, Z. Li, X. Luo, Materials Science and Engineering A 456 (2007) 43–51.
[15] Y.B. Chun, S.H. Yu, S.L. Semiatin, S.K. Hwang, Materials Science and Engineering A 398 (2005) 209–219.
[16] V.M. Segal, Materials Science and Engineering A 197 (1995) 157–164.
[17] V.M. Segal, K.T. Hartwig, R.E. Goforth, Materials Science and Engineering A 224 (1997) 107–115.
[18] K. Máthis, J. Gubicza, N.H. Nam, Journal of Alloys and Compounds 394 (2005) 194–199.
[19] H.K. Kim, Y.I. Lee, C.S. Chung, Scripta Materialia 52 (2005) 473–477.
[20] M. Eddahbi, P. Pérez, M.A. Monge, G. Garcés, R. Pareja, P. Adeva, Journal of Alloys and Compounds 473 (2009) 79–86.
[21] G. Ben Hamu, D. Eliezer, L. Wagner, Journal of Alloys and Compounds 468 (2009) 222–229.
[22] B. Chen, D.L. Lin, L. Jin, X.Q. Zeng, C. Lu, Materials Science and Engineering A 483–484 (2008) 113–116.
[23] Y. Iwahashi, Z. Horita, M. Nemoto, T.G. Langdon, Acta Materialia 46 (1998) 3317–3331.
[24] W.J. Kim, S.I. Hong, Y.S. Kim, S.H. Min, H.T. Jeong, J.D. Lee, Acta Materialia 51 (2003) 3293–3307.
[25] N. Balasubramani, A. Srinivasan, U.T.S. Pillai, K. Raghukandan, B.C. Pai, Journal of Alloys and Compounds 455 (2008) 168–173.
[26] S.Y. Chang, S.W. Lee, K.M. Kang, S. Kamado, Y. Kojima, Materials Transactions 45 (2004) 488–492.
[27] K. Xia, J.T. Wang, X. Wu, G. Chen, M. Gurvan, Materials Science and Engineering A 410–411 (2005) 324–327.
[28] M. Janeček, M. Popov, M.G. Krieger, R.J. Hellmig, Y. Estrin, Materials Science and Engineering A 462 (2007) 116–120.
[29] Z. Zuberova, Y. Estrin, T.T. Lamark, M. Janeček, R.J. Hellmig, M. Krieger, Journal of Materials Processing Technology 184 (2007) 294.
[30] A.A. Luo, Materials Science Forum 419–422 (2003) 57–66.
[31] K. Nakashima, Z. Horita, M. Nemoto, T.G. Langdon, Acta Materialia 5 (1998) 1589–1599.
[32] P.B. Berbon, T.G. Langdon, The Minerals, Metal and Materials society (2000) 381–392.
[33] C.W. Su, L. Lu, M.O. Lai, Materials Science and Engineering A 434 (2006) 227–236.
[34] M.H. Yoo, S.R. Agnew, J.R. Morris, K.M. Ho, Materials Science and Engineering A 319–321 (2001) 87–92.